research papers

Site preference and lattice relaxation around 4d and 5d refractory elements in Ni$_3$Al

Ana Umićević,[a]* Heinz-Eberhard Mahnke,[b,c] Jelena Belošević-Čavor,[a] Božidar Cekić,[a] Gerhard Schumacher,[b] Ivan Madjarevic[a] and Vasil Koteski[a]

[a]Vinča Institute of Nuclear Sciences, University of Belgrade, PO Box 522, Belgrade 11001, Serbia, [b]Helmholtz-Zentrum Berlin für Materialien und Energie GmbH, Hahn-Meitner-Platz 1, D-14109 Berlin, Germany, and [c]Fachbereich Physik, Freie Universität Berlin, Arnimallee 14, D-14195 Berlin, Germany. *Correspondence e-mail: umicev@vin.bg.ac.rs

X-ray absorption spectroscopy is employed to investigate site preference and lattice relaxation around Mo, Ru, Hf, W and Re dopants in Ni$_3$Al. The site occupation preference and the measured distances between the refractory elements as dopants and the nearest host atoms are compared with the results of *ab initio* calculations within the density functional theory. Combined experimental and theoretical results indicate that Mo, Hf, W and Re atoms reside on the Al sublattice in Ni$_3$Al, while Ru atoms occupy the Ni sublattice. A more pronounced lattice relaxation was detected in the case of Hf and Ru doping, with a strong outward relaxation of the nearest Ni and Al atoms.

1. Introduction

Nickel-based superalloys have been extensively studied due to their unmatched high-temperature strength and resistance to creep and oxidation. They are of great technological importance and are widely used in various industrial applications, including land-based and aerospace turbine engines. The origin of the high-temperature mechanical properties of these alloys can be found in the strengthening of the face-centered cubic Ni solid solution matrix (γ-phase) by coherent elastically hard γ'-phase (L1$_2$ Ni$_3$Al) precipitates. Refractory element additions such as Re, Ta or W are known to improve the corrosion resistance and mechanical properties of the Ni-based alloys (Giamei & Anton, 1985). Various refractory elements also improve the stability of the γ'-phase precipitate in the superalloy and provide solid-solution strengthening (Reed, 2006). By inducing distortions in the alloys, they can change the lattice mismatch between the two phases, which is believed to be an important parameter in the process of solid solution strengthening (Rüsing *et al.*, 2002). The site preference of the impurity atom in L1$_2$ Ni$_3$Al structure influences the diffusion behavior of components at high temperatures and therefore may have significant impact on Ni$_3$Al high-temperature properties (Gopal & Srinivasan, 2012). However, given that the multicomponent Ni-based superalloys are very complex, the actual role of the embedded elements is still under debate (for example, see Chen *et al.*, 2010; Carroll *et al.*, 2006; Yeh & Tin, 2006; Fleischmann *et al.*, 2015), and, in principle, it should be evaluated on a case-by-case basis. Therefore, the current optimization of the physical and mechanical properties of the Ni-based superalloys requires a detailed understanding of the site preference and lattice relaxation around the refractory elements embedded in the individual phases.
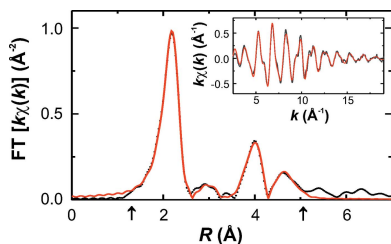
In our earlier paper (Koteski *et al.*, 2008), we have investigated the lattice relaxation around several important refractory elements incorporated in Ni (γ-phase). In this paper, we extend our investigation to the complementary Ni$_3$Al (γ'-phase). In Ni$_3$Al, in addition to the lattice relaxation around the impurity, the site preference of the impurity atoms is also *a priori* unknown. By means of X-ray absorption spectroscopy in combination with *ab initio* density functional theory calculations, we reveal the lattice site preference and relaxation effects in γ'-Ni$_3$Al containing 2 at.% Mo, Ru, Hf, W and Re providing a direct experimental and theoretical insight into the local structure close to the incorporated atoms.

2. Experimental methods

The γ'-Ni$_3$Al(X) (X = Mo, Ru, Hf, W, Re) samples with 2 at.% of alloying elements were produced from high-purity components in an induction furnace. The nickel, aluminium and element X were taken in stoichiometric proportions by weight with the nominal compositions Ni$_{73.5}$Al$_{24.5}$$X_2$ to obtain the alloys. The preparation of the Ni$_3$Al(X) alloys was carried out by first producing a pre-alloy: Ni + X (X = Mo, Ru, Hf, W or Re), and then adding aluminium to the alloys. The aluminium causes an oxide layer to form which prevents fast cooling. All alloying elements were introduced as larger pieces. To achieve good homogeneity, the ingots were turned upside down and remelted several times. To improve the homogeneity of the produced material, Ni$_3$Al(Ru) was subjected to additional heat treatment by keeping the sample at 1030°C for 24 h in argon atmosphere. With regard to the Ni$_3$Al(Ru) sample, a piece of non-melted metal was found in the part which was not measured by extended X-ray absorption fine-structure (EXAFS) spectroscopy. The composition of the Ni$_3$Al(Ru) alloy measured by EXAFS might, therefore, (slightly) deviate from the nominal composition.

The local structure around the impurity atoms was investigated by employing EXAFS spectroscopy at the X1 beamline of HASYLAB at DESY. We used a seven-segment Ge detector to measure the spectra in fluorescence mode. The fluorescence spectra were collected at the K absorption edges of Mo, Ru, Hf, W and Re. Using a liquid-helium cryostat, the temperature of the investigated samples was kept at 20 K [for Ni$_3$Al(X), X = Mo, Hf, W and Re] and 46 K [for Ni$_3$Al(Ru)]. The low-temperature measurements are important for obtaining good quality spectra because of the reduced 'dynamical damping' of the EXAFS signal. For the Ni$_3$Al(X) (X = Hf, W and Re) samples, the fluorescence spectra were also collected at 297 K. To obtain the EXAFS spectra, $\chi(k)$, after background subtraction, we used the *ATHENA* code (Ravel & Newville, 2005). The possible damping of the measured fluorescence intensity due to self-absorption effects was corrected by using the *ATOMS* algorithm (Ravel, 2001), as implemented in the *ATHENA* code. This correction affects only the amplitude of the measured EXAFS data (not the phase), so the data can be reliably analyzed for bond lengths. To prepare the fitting procedure, the $\chi(k)$ spectra were multiplied by k and Fourier-transformed into R-space. The

ab initio theoretical standards computed with the *FEFF9* code (Rehr *et al.*, 2010) were used in the fitting. The theoretical standards were obtained on a 135-atom cluster of pure γ'-Ni$_3$Al [L1$_2$-structure, a = 3.5718 Å, space group No. 221 (Rao *et al.*, 1989)], in which one atom (Ni or Al) in the cluster's interior was replaced with the corresponding impurity atom. Using the *FEFF* self-consistent potential calculation (SCF), the Fermi energy and charge transfer between the atoms in the cluster were calculated on an *ab initio* level. This enables better theoretical description of the EXAFS with smaller k-wavenumbers. The actual fitting was performed with the *ARTEMIS* software package (Ravel & Newville, 2005).

The data statistics collected around the Mo and Ru K-edge were found to be sufficient to include higher shells in the fits, while for Hf, W and Re only the first shell was fitted. For Mo and Ru, the fitting procedure included the first several single-scattering (SS) paths. The mean-square variations of the scattering path, σ^2, were fitted independently. In the K-edge *FEFF* calculations, several multiple scattering (MS) paths were found to have substantial contributions in the area around the fourth atomic shell. These paths were included in the fit of the Mo and Ru data. Their structural parameters were fitted independently. They were found to significantly improve the quality of the fits in the area around 5 Å.

To reduce the number of free variables and to improve the quality of the fits, we performed simultaneous data sets fitting of the 20 K and 297 K spectra for Ni$_3$Al(X), X = Hf, W and Re. The simultaneous fitting was performed assuming linear temperature dependence and introducing coefficients of thermal expansion. The amplitude reduction term, S_0^2, and the energy shift parameter, E_0, were treated as independent variables in all data sets. All the fits presented in this paper were Fourier transformed using a Kaiser-Bessel window with a sill width of 1 Å^{-1}.

3. Numerical method

To calculate the interatomic distances, we used the all-electron augmented plane-wave plus local orbitals (APW + lo) code *Wien2k* (Blaha *et al.*, 1990, 2001). Starting from a fully relaxed γ'-Ni$_3$Al unit cell, we constructed a 2 × 2 × 2 supercell, in which one of the host atoms was replaced by the impurity. The entire supercell was then allowed to relax in accordance with the Hellmann–Feynman forces until the forces were smaller than 5 mRy a.u.$^{-1}$. This 32-atom supercell corresponds to an impurity concentration of $\sim$3.1% [Ni$_{71.875}$$X_{3.125}Al_{25}$ or Ni$_{75}$Al$_{21.875}$$X_{3.125}$ (X = Mo, Ru, Hf, W, Re)] and a fixed impurity–impurity distance of 7.138 Å. The $R_{mt}K_{max}$ parameter, which determines the size of the basis set, was set to 8. The radii of the non-overlapping muffin-tin (MT) spheres around the atoms were set to 2.4 a.u. for Re and W; 2.3 a.u. for Hf, Mo and Ru; 2.2 a.u. for Ni; and 2.1 a.u. for Al. We used a threshold energy of −7 Ry to separate the core and valence states. The k-space integration was performed by using the tetrahedron method, with as many as 40 k-points in the irreducible part of the Brillouin zone (8 × 8 × 8 k-mesh). To describe the exchange and correlation effects between the

electrons, we used the generalized gradient approximation parametrized by Perdew–Burke–Ernzerhof (Perdew *et al.*, 1996).

The site preference of the investigated impurities in γ'-Ni$_3$Al can be assessed *via* the isolated point defects formation energies. The defect formation energies were calculated according to the relation

$$E_{\text{form}} = E_{\text{d}} - E_{\text{pure}} + \sum n_i \mu_i, \qquad (1)$$

where E_{d} is the total energy of the supercell with the substituted impurity, E_{pure} is the total energy of the supercell without the impurity, μ_i is the chemical potential of the species of type i (in our case, the energy per atom obtained from the corresponding metal phases of Mo, Ru, W, Hf, Re, Ni and Al), and n_i is the number of atoms of type i added to, or removed from, the supercell.

For the calculation of defect energies, we employed the much faster projector augmented-wave (PAW) code *VASP* (Kresse & Joubert, 1999; Kresse & Furthmüller, 1996). To test the convergence of the calculated defect energies, in addition to the supercell described above, we used a larger $3 \times 3 \times 3$ supercell of 108 atoms [Ni$_{74.074}$X$_{0.926}$Al$_{25}$ or Ni$_{75}$Al$_{24.074}$X$_{0.926}$ (X = Mo, Ru, Hf, W, Re)]. Our calculations were spin-polarized, with a cutoff energy of 300 eV, $10 \times 10 \times 10$ k-point mesh for the smaller and $4 \times 4 \times 4$ k-points for the larger supercell, and a force convergence criterion of 0.02 eV Å^{-1}.

4. Experimental results

4.1. 4d elements Mo and Ru in Ni$_3$Al

The k-weighted EXAFS spectrum of Mo-doped Ni$_3$Al (2 at.% of Mo) collected at the Mo K-edge at 20 K and its Fourier transform are given in Fig. 1. The best fit (R-factor 0.84%) was obtained for the Mo(Al) structure model. In this model, Mo substitutes for Al in the Ni$_3$Al crystal lattice. The first coordination shell consists of 12 Ni atoms, *i.e.* there are 12 nearest neighbor (NN) nickel atoms. There are 6 Al atoms in the second [6 next nearest neighbor (NNN) Al atoms], 24 Ni atoms in the third, and 12 Al atoms in the fourth coordination
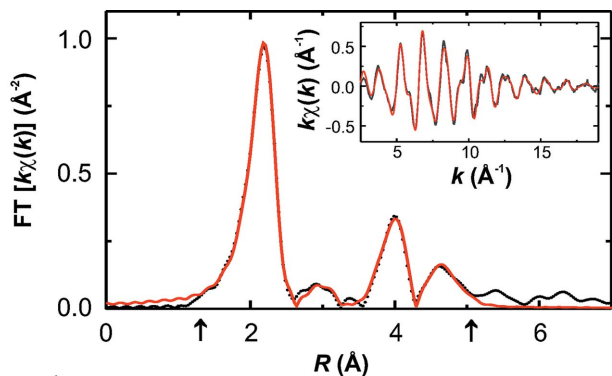
Table 1
Ni$_3$Al:Mo: fitted values from EXAFS data for the energy shift E_0, the amplitude reduction term S_0^2, Debye–Waller factors σ^2 and interatomic distances R for the first four coordination shells around Mo on the Al site in Ni$_3$Al.

The coordination numbers are fixed to the values of the pure compound. The fit ranges ΔR and Δk are also indicated. The errors given in parentheses are from the fitting procedure only.

	R_{I} (Å)	R_{II} (Å)	R_{III} (Å)	R_{IV} (Å)
Mo—Ni	2.527 (1)		4.391 (5)	
Mo—Al		3.58 (2)		5.15 (2)

	σ_{I}^2 (Å^2)	σ_{II}^2 (Å^2)	σ_{III}^2 (Å^2)	σ_{IV}^2 (Å^2)
Mo—Ni	0.0022 (1)		0.0037 (4)	
Mo—Al		0.010 (6)		0.1 (1)

E_0 (eV)	S_0^2	ΔR (Å)	Δk (Å^{-1})
2.1 (4)	0.80 (1)	1.30–5.05	2.45–18.00

shell around Mo. The coordination numbers of all the paths in our fit were fixed to their corresponding values in the pure compound. We fitted the first four SS paths, Mo–Ni1 (R_{I}), Mo–Al1 (R_{II}), Mo–Ni2 (R_{III}) and Mo–Al2 (R_{IV}), as well as four additional MS paths with contributions between 3.7 and 5.1 Å. As can be seen, there is a relatively good agreement between the experimental data and our model. The values of the complete set of fitted parameters are given in Table 1.

The k-weighted EXAFS spectrum of Ru-doped Ni$_3$Al (2 at.% of Ru) collected at the Ru K-edge at 46 K and its Fourier transform are presented in Fig. 2. The fit was obtained with the model where Ru substitutes for Ni in the crystal lattice of Ni$_3$Al. In this model, the first and third shell around Ru are divided into two Ni and Al subshells. We fitted the first six SS paths, Ru–Ni1 (R_{I}), Ru–Al1 (R_{I}), Ru–Ni2 (R_{II}), Ru–Ni3 (R_{III}), Ru–Al2 (R_{III}) and Ru–Ni4 (R_{IV}), as well as two additional MS paths with contributions around 5.1 Å. The coordination numbers of all the paths in our fit were fixed to their corresponding values in the pure compound. A relatively good agreement between the experimental data and our model was obtained, as reflected in the value of the R-factor of 1.14%.

Figure 1
Fourier transform of the EXAFS oscillations of the Ni$_3$Al:Mo sample (dotted line) and fit (solid line). The corresponding k-weighted EXAFS spectrum is given in the inset. The fit range ΔR is marked by arrows.
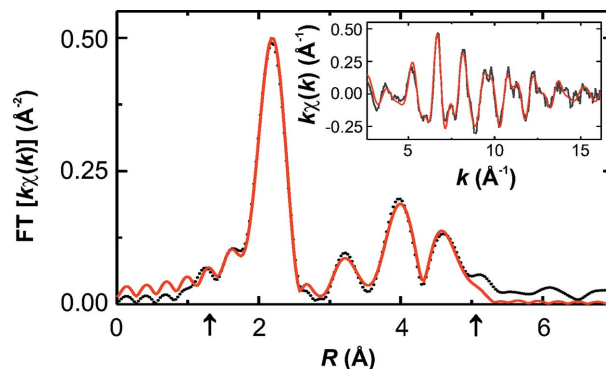
Figure 2
Fourier transform of the EXAFS oscillations of the Ni$_3$Al:Ru sample (dotted line) and fit (solid line). The corresponding k-space spectrum is given in the inset. The fit range ΔR is marked by arrows.

Table 2
Ni₃Al:Ru: fitting parameters used for the first four coordination shells around Ru on the Ni site in Ni₃Al.

For definition of symbols see Table 1. The coordination numbers were fixed to the values of the pure compound.

	R_I (Å)	R_{II} (Å)	R_{III} (Å)	R_{IV} (Å)
Ru—Ni	2.539 (6)	3.56 (3)	4.38 (2)	5.1 (1)
Ru—Al	2.62 (4)		4.37 (8)	
	σ_I^2 (Å²)	σ_{II}^2 (Å²)	σ_{III}^2 (Å²)	σ_{IV}^2 (Å²)
Ru—Ni	0.0019 (4)	0.008 (3)	0.002 (1)	0.000 (9)
Ru—Al	0.016 (8)		0.01 (2)	

E_0 (eV)	S_0^2	ΔR (Å)	Δk (Å⁻¹)
−2 (1)	0.71 (2)	1.30–5.05	2.65–12.95

The values of the complete set of fitted parameters are given in Table 2.

4.2. 5d elements Hf, W and Re in Ni₃Al

The statistics of the data collected for Ni₃Al doped with Hf, W and Re were such that we could fit only the area around the first dominant peak. Because the EXAFS data were collected at two different temperatures, 20 K and 297 K, we were able to perform simultaneous multiple data sets fitting. By fitting multiple data sets, we were able to reduce the correlation between the fit parameters and obtain more accurate fits. In this case, our fitting model accommodates different S_0^2, E_0 and σ^2 parameters for the scattering paths in both data sets. The ΔR parameters, however, were mutually related via the thermal expansion coefficients, α and β, as follows: $\Delta R(T) = (\alpha T + \beta)R_{eff}$. Here, R_{eff} is the initial half path length of the corresponding single-scattering path and ΔR is the change in the initial half path length.

Given the limited R-space (the area around the first dominant peak), we found that both fitting models fit the 5d elements EXAFS data with comparable accuracy. The difference between the models is that, when the impurity substitutes on the Ni lattice site, the first atomic shell of 12 Ni atoms is divided into two subshells with 8 Ni and 4 Al atoms. FEFF calculations for dopants on the Ni sublattice indicated that the contribution of the Al subshell in the first peak area is much smaller and overlaps with the Ni contribution in the same area. The analysis of these two contributions showed that the inclusion of the Al subshell reduces the intensity of the first-shell peak due to interference. Also, it was noted in some previous XAFS measurements at the K-edges of 3d dopants in Ni₃Al that the aluminium contribution was difficult to detect in the EXAFS [Balasubramanian et al., 1997a (Fe, Co); Balasubramanian et al., 1997b (Ti, V, Cr, Mn, Fe, Co); Lawniczak-Jablonska et al., 1992 (Fe); Pascarelli et al., 1994 (Fe)]. The structural disorder introduced in Ni₃Al by these dopants was provided as a possible explanation. This was found to be especially important in the case of Co dopant occupying the Ni sublattice in Ni₃Al (Balasubramanian et al.,

Table 3
Ni₃Al:Hf: fitted values from EXAFS data for the energy shift E_0, the amplitude reduction term S_0^2, Debye–Waller factors σ^2, and interatomic distances R for the first coordination shell around Hf on the Al site in Ni₃Al.

The coordination number was fixed to the value of the pure compound. The fit ranges ΔR and Δk are also indicated. The errors given in parentheses are from the fitting procedure only.

	Hf—Ni	
	$T = 20$ K	$T = 297$ K
R_I (Å)	2.580 (5)	2.58 (1)
σ_I^2 (Å²)	0.0016 (4)	0.0021 (8)
E_0 (eV)	−3 (2)	−4 (2)
S_0^2	0.90 (9)	0.8 (1)
ΔR (Å)	1.300–2.526	1.300–2.526
Δk (Å⁻¹)	2.50–15.54	2.90–11.55

1997a) where a large structural disorder on the Al sublattice implied the total absence of Al backscattering contributions in the first peak signal. Therefore, from the EXAFS data alone, we are unable to exclude the possibility of substitution on the complementary lattice site. In the following, we present the fit with slightly better R-factor for Hf(Al), and for W and Re, where our theoretical calculations suggested that the models with a slightly worse R-factor, W(Al) and Re(Al), should be preferred over the W(Ni) and Re(Ni) models.

The Fourier-transformed k-weighted EXAFS spectra of Hf-doped Ni₃Al (2 at.% of Hf) collected around the Hf K-edge at 20 K and 297 K are presented in Fig. 3. Also, in the inset, the corresponding $k\chi(k)$ oscillations are given. The best fit (R-factor 0.96%) was obtained for the Hf(Al) structure model. In this model, the first shell consists of 12 Ni atoms. The results of the fit are presented in Table 3.

Fig. 4 depicts the Ni₃Al:W (2 at.% tungsten concentration) Fourier-transformed k-weighted EXAFS spectrum collected at the W K-edge at 20 K and 297 K. The W(Al) structure model, containing 12 Ni atoms in the first shell, produced a fit with an R-factor of 1.29%. The values of the fitted parameters
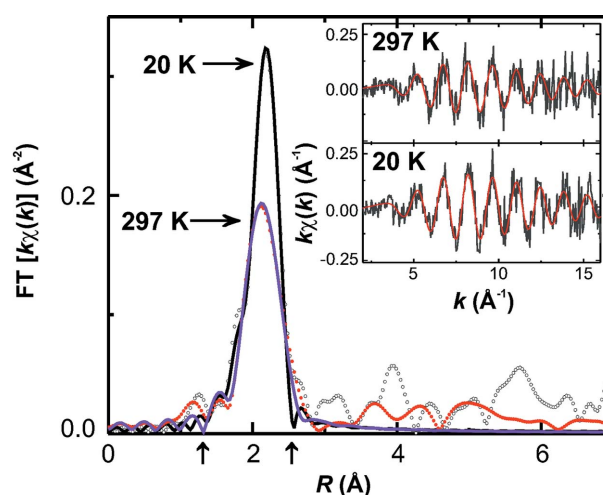
Figure 3
Fourier transforms of the EXAFS oscillations of the Ni₃Al:Hf sample (dotted lines) and fit (solid lines). The corresponding k-weighted EXAFS spectra are given in the inset. The fit range ΔR is marked by arrows.

Ana Umićević et al. · Site preference and lattice relaxation in Ni₃Al   **289**

Table 4
Ni$_3$Al:W: fitting parameters used for the first coordination shell around W on the Al site in Ni$_3$Al.

For definition of symbols see Table 3. The coordination number was fixed to the value of the pure compound.

	W—Ni	
	$T = 20$ K	$T = 297$ K
R_I (Å)	2.522 (7)	2.51 (2)
σ_I^2 (Å^2)	0.0009 (2)	0.0037 (6)
E_0 (eV)	0 (2)	−3 (5)
S_0^2	0.70 (2)	0.70 (3)
ΔR (Å)	1.300–2.526	1.300–2.526
Δk (Å^{-1})	3.00–15.90	5.40–11.77

Table 5
Ni$_3$Al:Re: fitted values from EXAFS data for the first coordination shell around Re on the Al site in Ni$_3$Al.

For definition of symbols see Table 3. The coordination number was fixed to the value of the pure compound.

	Re—Ni	
	$T = 20$ K	$T = 297$ K
R_I (Å)	2.499 (6)	2.50 (2)
σ_I^2 (Å^2)	0.0005 (3)	0.0030 (5)
E_0 (eV)	0 (2)	−2 (4)
S_0^2	0.70 (3)	0.70 (2)
ΔR (Å)	1.300–2.526	1.300–2.526
Δk (Å^{-1})	3.25–14.85	2.85–13.40
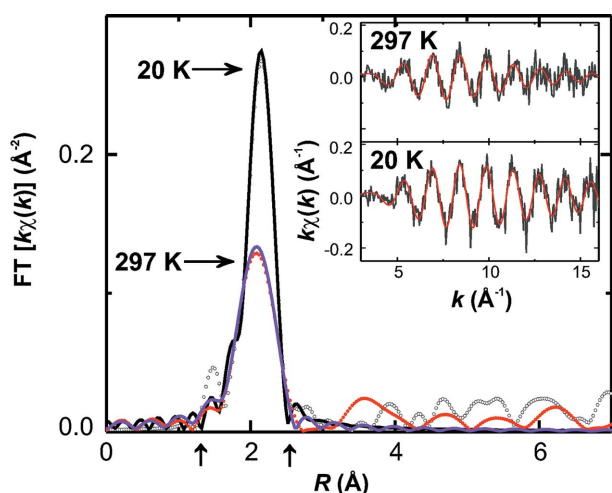
Figure 4
Fourier transforms of the EXAFS oscillations of the Ni$_3$Al:W sample (dotted lines) and fit (solid lines). The corresponding k-space spectra are given in the inset. The fit range ΔR is marked by arrows.
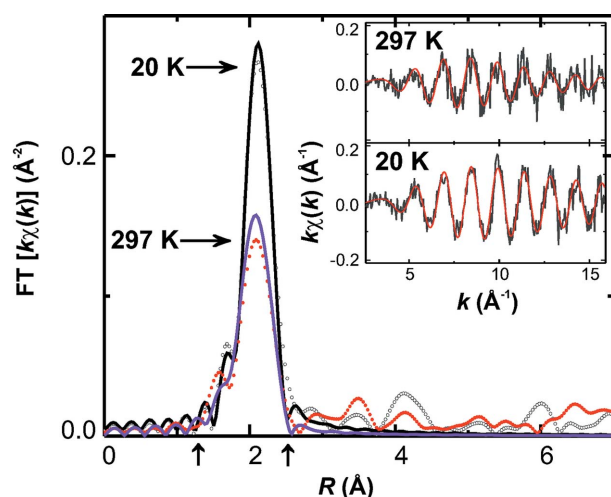
Figure 5
Fourier transforms of the EXAFS oscillations of the Ni$_3$Al:Re sample (dotted lines) and fit (solid lines). The corresponding k-weighted EXAFS spectra are given in the inset. The fit range ΔR is marked by arrows.

are given in Table 4. The Fourier-transformed k-weighted EXAFS spectra of Re-doped Ni$_3$Al (2 at.% of Re) at the Re K-edge at 20 K and 297 K are presented in Fig. 5. The fit with R-factor of 2.89% was obtained for the structure model where Re substitutes for Al (the first shell of 12 Ni atoms). The results of the fit are presented in Table 5.

5. Discussion

Tables 6 and 7 comprise the calculated (*WIEN2k*) NN bond lengths between the dopant (situated on Ni or Al lattice site) and the nearest host atoms. The calculated bond lengths, as extracted from the 32-atom supercell, correspond to a concentration of ~3.1 at.% of refractory atoms in Ni$_3$Al, which matches relatively well the experimental impurity concentration of 2 at.%. Our calculations predict that the largest lattice relaxation should be expected in the case of Hf doping, regardless of the actual site occupancy. For Hf substituting on Al, there is an outward relaxation of ~2.77%. For Hf substituting on Ni, the outward relaxation of the NN Ni atoms is somewhat reduced (1.47%), but the four atoms in the Al subshell are moved from their original positions by

~7.17%, which is the largest calculated relaxation amongst the investigated impurities.

Based on our *WIEN2k* calculations, when the dopants substitute on the Ni lattice site the four NN Al atoms should exhibit outward relaxation. Outward relaxation is also predicted for the NN Ni atoms around Ru, Hf and Re, whereas the Mo—Ni and W—Ni bond lengths are somewhat reduced. When the dopants substitute on the Al lattice site, there is an inward relaxation of the NN Ni shell around Ru and Re. By contrast, Mo, Hf and W tend to push the NN Ni atoms away from their original positions.

The values of the defect formation energies of Mo, Ru, Hf, W and Re, as calculated with the *VASP* code, are given in Table 8. The convergence of the calculated formation energies was checked with a larger 108-atom supercell that corresponds to an average dopant concentration of ~0.93%. As can be seen, the calculated energies are relatively well converged. Lower formation energies are obtained in the case of Al-site substitution for all of the investigated refractory elements, except for Ru, where, clearly, the Ni lattice site substitution is preferred.

According to the results of our Mo and Ru EXAFS analysis, Mo substitutes on Al, whereas Ru occupies the Ni lattice site.

Table 6
Calculated NN distances between the central refractory atom at the Ni site and the first shell host atoms in Ni_3Al.

For pure Ni_3Al, for relaxed structure, the calculated NN distance is 2.524 Å.

	I Ni-subshell 8(Ni) $X-Ni$ (Å)	I Ni-subshell relaxation (% of calc for pure Ni_3Al)	I Al-subshell 4(Ni) $X-Al$ (Å)	I Al-subshell relaxation (% of calc for pure Ni_3Al)
Mo	2.512	−0.48	2.675	+6.00
Ru	2.541	+0.67	2.589	+2.58
Hf	2.561	+1.47	2.705	+7.17
W	2.509	−0.59	2.675	+5.98
Re	2.529	+0.20	2.625	+4.00

Table 7
Calculated NN distances between the central refractory atom at the Al site and the first shell host atoms in Ni_3Al.

For pure Ni_3Al, for relaxed structure, the calculated NN distance is 2.524 Å.

	I Ni-shell 12(Ni) $X-Ni$ (Å)	I shell relaxation (% of calc for pure Ni_3Al)
Mo	2.534	+0.40
Ru	2.514	−0.40
Hf	2.594	+2.77
W	2.534	+0.40
Re	2.514	−0.40

Table 8
Defect formation energies of Mo, Ru, Hf, W and Re dopants in Ni_3Al.

System	E_{form} (eV) $2 \times 2 \times 2$ supercell	E_{form} (eV) $3 \times 3 \times 3$ supercell
Mo(Ni)	1.08	1.10
Mo(Al)	0.87	0.91
Ru(Ni)	0.92	0.88
Ru(Al)	2.05	1.95
Hf(Ni)	0.12	0.04
Hf(Al)	−0.33	−0.14
W(Ni)	1.03	1.05
W(Al)	0.62	0.69
Re(Ni)	1.19	1.25
Re(Al)	1.03	1.09

This is in agreement with the site preference predicted by our total energy calculations. Additional confirmation comes from comparing the shape of the Mo and Ru Fourier-transformed spectra in the region around 3.3 Å. For Ru, there is a prominent peak in this region, but one is lacking in the Mo spectrum. This peak has also been previously associated with Ni-site substitution for different 3d doping atoms (Sakurai *et al.*, 1997). The origin of this peak is actually in the scattering from the second atomic shell. If the impurity substitutes on the Ni lattice site, the second atomic shell around the impurity contains six Ni atoms. When the impurity is on the Al lattice site, the second atomic shell is comprised of six Al atoms. For 4d and 5d dopants in Ni_3Al investigated in this work, the *FEFF* calculations indicate that this peak should be prominent only in the case of Ni lattice site substitution, and, at the same time, it is an indication of Ni site preference. Unfortunately, we could not use this argumentation for the 5d impurities,

where the quality of the EXAFS signal beyond the first atomic shell was rather poor.

For the case of Hf dopants, the best EXAFS fit was obtained with the Al-site substitution model. This site preference agrees with our numerical calculations. For W and Re, the Ni-site substitution models were somewhat more successful in fitting the EXAFS data. However, the fitted first shell W−Al bond length of 2.576 Å was too far away from the calculated bond length of 2.675 Å. The discrepancy between the measured and calculated W−Al distance, along with the lower defect formation energy of W on the aluminium lattice site, indicated that the W(Al) fitting model should be adopted as more relevant for tungsten in Ni_3Al despite the somewhat higher value of the *R*-factor. The same arguments were applied when we decided to dismiss the Re(Ni) model for the Ni_3Al:Re EXAFS fit, since the fitted first-shell Re−Ni bond length of 2.503 Å was too far from the calculated value of 2.523 Å. Also, the higher defect formation energy of Re on the Ni site suggested that we should adopt the Re(Al) model.

It should be noted that EXAFS measures the local distances from the absorbing atom (*e.g.* Mo, Ru, Hf, W or Re) to the neighbor atoms (NN atoms, NNN atoms, *etc.*). The NN and NNN distances presented in Tables 1–5 should be distinguished from the interatomic distances obtained by X-ray diffraction (Mishima *et al.*, 1985). For example, for the W absorbing atom positioned at the Ni site in the Ni_3Al lattice, EXAFS examines only W−Ni NN distances. As the concentration of the substituting atom is small, most of the Ni sites in the Ni_3Al:W lattice are occupied by Ni atoms. The addition of W atoms will globally cause a change (*i.e.* expansion) of the lattice parameter as measured by X-ray diffraction (XRD) (Mishima *et al.*, 1985), but XRD cannot probe an actual local distortion (*i.e.* shrinkage, see Table 4) of the lattice around W atoms, since XRD provides only the averaged superposition of W−Ni, Ni−Ni and Ni−Al NN distances.

A comparison between the calculated NN distances and the distances extracted from the EXAFS fits is depicted in Fig. 6. As can be seen, our calculations reproduce the experimental trends relatively well. Among the investigated dopants, the Mo−Ni, Ru−Ni and Hf−Ni bonds are elongated by ∼0.04, 0.51 and 2.14%, respectively, with respect to the pure Ni_3Al value [Ni−Ni bond of 2.526 Å (Rao *et al.*, 1989)], while the W−Ni and Re−Ni bonds are shortened by ∼0.16 and 1.07%, respectively. In the case of Ru, which occupies the Ni lattice position, the Ru−Al bond is elongated by ∼3.72%.

Our numerical results agree very well with the first-principles calculations of Ruban & Skriver (1997) who found strong Mo, Hf, W and Re preference and weak Ru preference for Al-site substitution in Ni_3Al. Experimental and calculation findings on Mo and Ru alloying effects and site preferences in Ni_3Al presented in this work are in agreement with the first-principle study of Geng *et al.* (2004). They have predicted that the Mo atom prefers the Al site and its NN and NNN atoms are almost completely undisturbed, while the Ru atom resides on the Ni site and its first-shell interatomic distances Ru−Ni and Ru−Al are variously extended. Jiang *et al.* (2006) used the first-principles supercell approach to calculate the Pt, Hf,
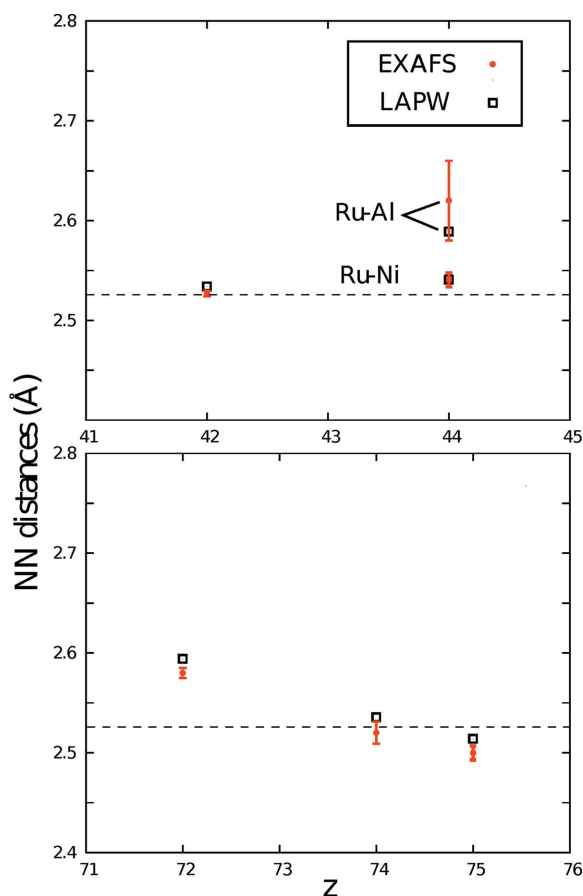
Figure 6
Comparison between the calculated (open squares) and measured (circles) NN bond lengths. For Ru Ni-site substitution the Ru—Al and Ru—Ni bond lengths of the NN shell are given separately. The horizontal dashed line denotes the Ni—Al distances in pure Ni₃Al.

Cr and Ir site preference. They found that, at 0 K, Hf always prefers Al lattice sites, which also agrees with our experimental and theoretical findings. The results of our formation energy calculations also agree with the results of the *ab initio* calculations of Zhou *et al.* (2008) for site occupation of Re, but strongly disagree for Ru. Using 32-atom supercell calculations, they have found lower defect formation energy of Ru on Al, in contrast to our results. The reason for this discrepancy is most likely the different functionals used in their study. The generalized gradient approximation functionals used in this work are known to predict binding energies and relative stabilities of solids much better than the local density approximation functionals.

6. Conclusion

We have used EXAFS measurements in combination with the density functional theory first-principles calculations to determine the site preference and lattice relaxation around Mo, Ru, Hf, W and Re dopants in Ni₃Al. Our results show that Mo, Hf, W and Re predominantly occupy the Al sublattice, whereas Ru has a strong preference for the Ni-site substitu-

tion. Our results indicate more pronounced outward lattice relaxation around Ru and Hf, whereas the lattice relaxation around Mo, W and Re is less distinct. We found excellent agreement between the measured and calculated bond lengths.

References

Balasubramanian, M., Lyver, R., Budnick, J. I. & Pease, D. M. (1997a). *Appl. Phys. Lett.* **71**, 330–332.
Balasubramanian, M., Lyver, R., Budnick, J. I. & Pease, D. M. (1997b). *J. Phys. IV Fr.* **7**, C2-1043–C2-1045.
Blaha, P., Schwarz, K., Madsen, G. K. H., Kvasnicka, D. & Luitz, J. (2001). *WIEN2k, An Augmented Plane Wave + Local Orbitals Program for Calculating Crystal Properties.* Karlheinz Schwarz, Technische Universität Wien, Austria.
Blaha, P., Schwarz, K., Sorantin, P. & Trickey, S. (1990). *Comput. Phys. Commun.* **59**, 399–415.
Carroll, L., Feng, Q., Mansfield, J. & Pollock, T. (2006). *Met. Mater. Trans. A*, **37**, 2927–2938.
Chen, J., Feng, Q. & Sun, Z. (2010). *Scr. Mater.* **63**, 795–798.
Fleischmann, E., Miller, M. K., Affeldt, E. & Glatzel, U. (2015). *Acta Mater.* **87**, 350–356.
Geng, C. Y., Wang, C. Y. & Yu, T. (2004). *Acta Mater.* **52**, 5427–5433.
Giamei, A. & Anton, D. (1985). *Metall. Trans. A*, **16**, 1997–2005.
Gopal, P. & Srinivasan, S. G. (2012). *Phys. Rev. B*, **86**, 014112.
Jiang, C., Sordelet, D. & Gleeson, B. (2006). *Acta Mater.* **54**, 1147–1154.
Koteski, V., Mahnke, H.-E., Belošević-Čavor, J., Cekić, B. & Schumacher, G. (2008). *Acta Mater.* **56**, 4601–4607.
Kresse, G. & Furthmüller, J. (1996). *Phys. Rev. B*, **54**, 11169–11186.
Kresse, G. & Joubert, D. (1999). *Phys. Rev. B*, **59**, 1758–1775.
Lawniczak-Jablonska, K., Pascarelli, S., Boscherini, F. & Kozubski, R. (1992). *Acta Phys. Pol.* A**82**, 315–322.
Mishima, Y., Ochiai, S. & Suzuki, T. (1985). *Acta Metall.* **33**, 1161–1169.
Pascarelli, S., Boscherini, F., Mobilio, S., Lawniczak-Jablonska, K. & Kozubski, R. (1994). *Phys. Rev. B*, **49**, 14984–14990.
Perdew, J. P., Burke, K. & Ernzerhof, M. (1996). *Phys. Rev. Lett.* **77**, 3865–3868.
Rao, P. V. M., Suryanarayana, S. V., Murthy, K. S. & Naidu, S. V. N. (1989). *J. Phys. Condens. Matter*, **1**, 5357–5361.
Ravel, B. (2001). *J. Synchrotron Rad.* **8**, 314–316.
Ravel, B. & Newville, M. (2005). *J. Synchrotron Rad.* **12**, 537–541.
Reed, R. C. (2006). *The Superalloys: Fundamentals and Applications.* New York: Cambridge University Press.
Rehr, J. J., Kas, J. J., Vila, F. D., Prange, M. P. & Jorissen, K. (2010). *Phys. Chem. Chem. Phys.* **12**, 5503–5513.
Ruban, A. V. & Skriver, H. L. (1997). *Phys. Rev. B*, **55**, 856–874.
Rüsing, J., Wanderka, N., Czubayko, U., Naundorf, V., Mukherji, D. & Rösler, J. (2002). *Scr. Mater.* **46**, 235–240.
Sakurai, M., Matsuura, M., Suzuki, K., Chiba, A. & Hanada, S. (1997). *J. Phys. IV Fr.* **7**, C2-1239–C2-1240.
Yeh, A. & Tin, S. (2006). *Met. Mater. Trans. A*, **37**, 2621–2631.
Zhou, Y., Mao, Z., Booth-Morrison, C. & Seidman, D. N. (2008). *Appl. Phys. Lett.* **93**, 171905.